Research Article

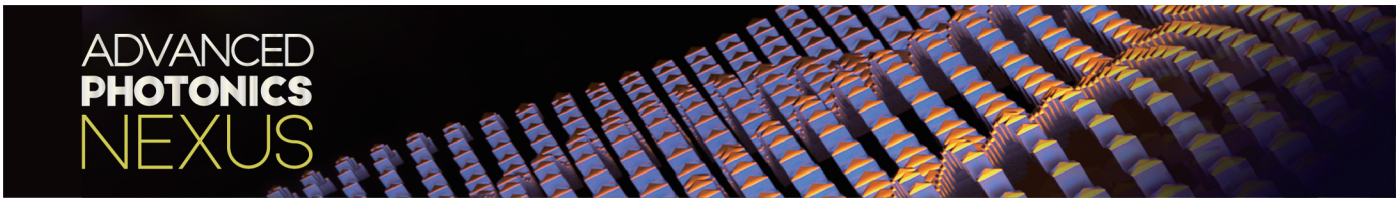

Hybrid silicon-barium-titanate tunable racetrack resonators based on chemical solution deposition

Lei Zhang,[a] Xin Wang,[a] Yong Zhang,[a,b,*] Jian Shen,[a] Chenglong Feng,[a] Jian Xu,[c] Min Liu,[c] Wei Wang,[d] Yongqiang Deng,[e] Yang Xu,[e] Yi Li,[e] Guofeng Yin,[f] and Yikai Su[a]

[a]Shanghai Jiao Tong University, State Key Lab of Advanced Optical Communication Systems and Networks, Department of Electron Engineering, Shanghai, China
[b]East China Normal University, State Key Laboratory of Precision Spectroscopy, Shanghai, China
[c]Shanghai Jiao Tong University, Center for Advanced Electronic Materials and Devices, Shanghai, China
[d]Shanghai Industrial μTechnology Research Institute, Shanghai, China
[e]Beijing R&D Institute, VanJee Technology, Beijing, China
[f]Wuhan Enlarging Photonics Technology Co. Ltd., Wuhan, China

Abstract. Integrated electro-optic tuning devices are essential parts of optical communication, sensors, and optical machine learning. Among the available materials, silicon is the most promising for on-chip signal processing and networks. However, silicon is limited owing to the absence of efficient Pockels electro-optic tuning. Herein, we propose a new hybrid silicon-barium-titanate (Si-BTO) integrated photonic platform, in which the BTO thin film is deposited by the chemical solution deposition (CSD) method. A tunable racetrack resonator is demonstrated to confirm the Pockels electro-optic tuning potential of the BTO thin film. The hybrid racetrack resonator has a tuning efficiency of 6.5 pm/V and a high-power efficiency of 2.16 pm/nW. Moreover, the intrinsic quality factor of the fabricated racetrack resonator is 48,000, which is the highest in hybrid Si-BTO platforms, to the best of our knowledge. The high-speed test verifies the stability of the racetrack resonator. The hybrid Si-BTO technology based on the CSD method has the advantages of low equipment cost and simple fabrication process, which holds promise for low-power electro-optic tuning devices.

Keywords: barium titanate; chemical solution deposition; electro-optic tuning; resonator.

Received Jun. 7, 2024; revised manuscript received Aug. 15, 2024; accepted for publication Sep. 24, 2024; published online Oct. 22, 2024.

[DOI: 10.1117/1.APN.3.6.066005]

1 Introduction

Photonic integrated circuits (PICs) are the fundamental building blocks for the implementation of optical neural networks,[1] quantum photonics,[2] optical communications,[3,4] and other applications. Tuning the effective refractive index of the input optical signal is a vital functionality needed in PICs. Such tuning function is used in many key components of PICs, such as electro-optic (EO) modulators[5,6] and switches.[7,8] Silicon-based tuning devices based on thermo-optic (TO) and free-carrier plasma dispersion (FCPD) effects have been investigated on account of high mode confinement and complementary metal-oxide-semiconductor (CMOS)-compatible fabrication processes.[9,10] However, both TO and FCPD effects have high power consumption, owing to their requirements of considerable current flow.[11] The Pockels effect, which is known as a linear EO effect, is a highly promising mechanism for developing low-power tuning devices. Based on the Pockels effect, several platforms, such as lithium niobate ($LiNbO_3$, LN),[12] lithium tantalite ($LiTaO_3$, LT),[13] and lead zirconate titanate (PZT)[14] have been explored. Among these, barium titanate (BTO) stands out as a promising material for the realization of EO tuning devices, attributed to its

*Address all correspondence to Yong Zhang, yongzhang@sjtu.edu.cn

Pockels coefficient of as high as 923 pm/V in a single-crystalline phase.[15]

Typically, methods for depositing BTO films are physical or chemical vapor deposition techniques.[16] These methods include molecular beam epitaxy (MBE),[17] pulsed laser deposition (PLD),[18] and radio-frequency (RF) sputtering.[19] Although some of these methods have been proven to produce high-quality BTO thin films, their deposition processes are complex. They require high vacuum conditions or precise temperature control,[15] and the equipment is expensive, with high maintenance costs.[20] Chemical solution deposition (CSD) has the advantages of low equipment cost, a simple fabrication process, and straightforward composition control,[15] which offers a fast and cost-effective method to realize CMOS-compatible EO devices.[16] Very recently, Picavet et al. introduced a method for integrating highly textured $BaTiO_3$ films by combining $La_2O_2CO_3$ template layers with CSD techniques. The reported Pockels coefficient (r_{eff}) reaches up to 139 pm/V, while the integrated BTO-SiN ring resonator modulator demonstrates a bandwidth exceeding 40 GHz.[21] The CSD-based Si-BTO integrated devices have not been reported yet. EO polymer materials prepared using the CSD method exhibit high EO coefficients and ultrafast response times, achieving bandwidths up to 500 GHz in plasmonic modulators.[22] However, these polymers cannot withstand the high temperatures required in silicon photonics, making them incompatible with CMOS processes. In addition, the issues of aging and long-term reliability of polymer materials cannot be overlooked.[23]

In our work, a hybrid Si-BTO integrated photonics platform is demonstrated using the CSD method. Based on our hybrid Si-BTO platform, a 70-μm-radius racetrack resonator is designed and fabricated. The fabricated racetrack resonator has an extinction ratio (ER) of 27.9 dB and a high intrinsic quality factor of 48,000. Benefiting from the strong Pockels effect in the BTO thin film, a tuning efficiency of 6.5 pm/V and a power efficiency of 2.16 pm/nW are obtained in the hybrid Si-BTO device. A high-speed transmission test of 50 Gbps nonreturn-to-zero (NRZ) signal indicates our device can support robust transmission of high-speed data. Our demonstration of a hybrid Si-BTO hybrid device, utilizing the CSD method, enables the integration of low-power EO tuning devices.

2 Materials and Methods

2.1 Device Design and Operation Principle

To make better utilization of the Pockels effect of the BTO thin film, a 100-nm-thick top silicon layer on a silicon-on-insulator (SOI) substrate is designed, which has a relatively thin thickness compared to traditional silicon waveguides. The silicon waveguide patterns are covered by a 150-nm-thick BTO thin film. The cross section of the hybrid Si-BTO waveguide is shown in Fig. 1(a). Since the refractive index of BTO (~2.3) is lower than that of silicon (~3.4), the 100-nm-thick silicon waveguides can not only guarantee the low propagation loss of light but also make good use of the great EO properties of BTO.

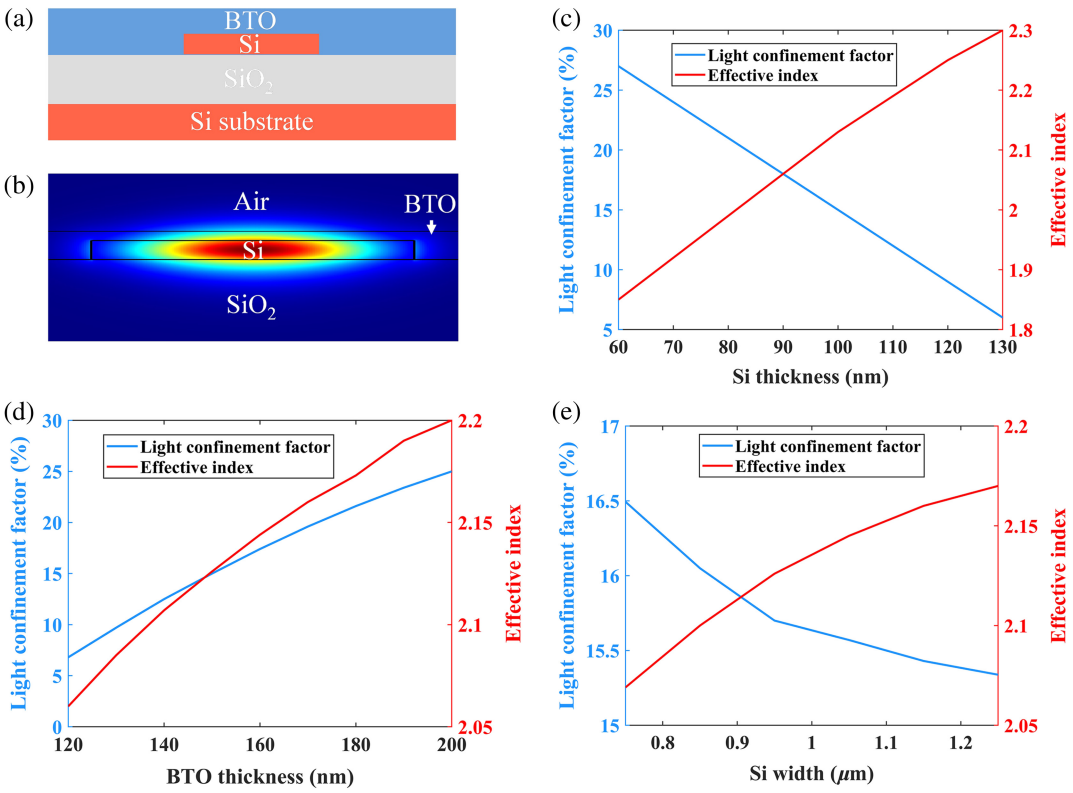

Fig. 1 (a) Cross section of the hybrid Si-BTO waveguide. (b) Simulated mode profile of the hybrid Si-BTO waveguide. (c) Simulated light confinement factor and effective index as a function of the thickness of the silicon layer. (d). Simulated light confinement factor and effective index as a function of the thickness of BTO thin film. (e) Simulated light confinement factor and effective index as a function of the width of the silicon layer.

Figure 1(b) shows the simulated transverse electric (TE) fundamental mode profile of the hybrid Si-BTO waveguide at 1550 nm. It can be found that the mode profile is confined in the silicon layer, and there is also a small amount of light leaking into the BTO layer above. We simulate the relationships between the mode properties and the waveguide parameters using the finite-element method, as shown in Figs. 1(c)–1(e). We can conclude that decreasing the thickness of the silicon layer effectively increases the proportion of light in the BTO film and results in a reduction in the effective mode index. The increase of the thickness of the BTO film shows increases in both light confinement and effective mode index. The changes in the width of silicon layers lead to little variation in the light confinement factor (from 15.2% to 16.5%). Taking all factors into account, the thickness of the silicon layer is 100 nm, the thickness of BTO is 150 nm, and the width of the silicon waveguide is 0.95 μm in our design. The light confinement in the BTO film is 15%, and the effective mode index is 2.13. The light confinement can be further improved by increasing the thickness of the BTO film. To implement Si-BTO devices with a standard 220-nm-thick SOI, we can reduce the waveguide width. This reduction would lessen the waveguide's confinement capability, thereby enhancing the optical field within the BTO film, enabling us to better leverage the film's exceptional EO properties.

To investigate the Pockels effect of the hybrid Si-BTO waveguide, we apply the electric field through gold microelectrodes beside the semicircle waveguides, as shown in Fig. 2(a). The simulated cross-sectional static electric field distribution is plotted in Fig. 2(b). We simulate the relationship between the average electric field and the electrode gap, as shown in Fig. 2(c). The average electric field can be calculated using the following equation:[24]

$$E_{\mathrm{avg}} = \frac{\iint_{\mathrm{BTO}} E_{x,op}^2 E_e \,\mathrm{d}x\,\mathrm{d}y}{\iint_{\mathrm{BTO}} E_{x,op}^2 \,\mathrm{d}x\,\mathrm{d}y}, \tag{1}$$

where $E_{x,op}$ and E_e represent the optical field and the electric field in the BTO, respectively. Existing studies indicate that the direction of the maximum EO coefficient is along r_{51}.[25] In our simulation, this direction is aligned parallel to the x axis of the cross-sectional electric field simulation diagram. Although the smaller electrode gap can achieve a better average electric field, the metal absorption needs to be considered at the same time. The effect of different silicon thicknesses and BTO thicknesses on the EO overlap factor is also simulated, as depicted in Fig. 2(d). The EO overlap factor is achieved by[24]

$$\Gamma = \frac{g}{v} \cdot E_{\mathrm{avg}}, \tag{2}$$

where v represents the applied voltage and g represents the electrode gap. The EO overlap factor declines when the thickness of silicon increases or the thickness of BTO decreases. When the silicon thickness is 100 nm, the EO overlap factor remains largely unaffected by variations in BTO thickness. To ensure the strong EO overlap and low metal absorption, the thickness of and the gap between the gold electrodes are 300 nm and 3 μm, respectively.

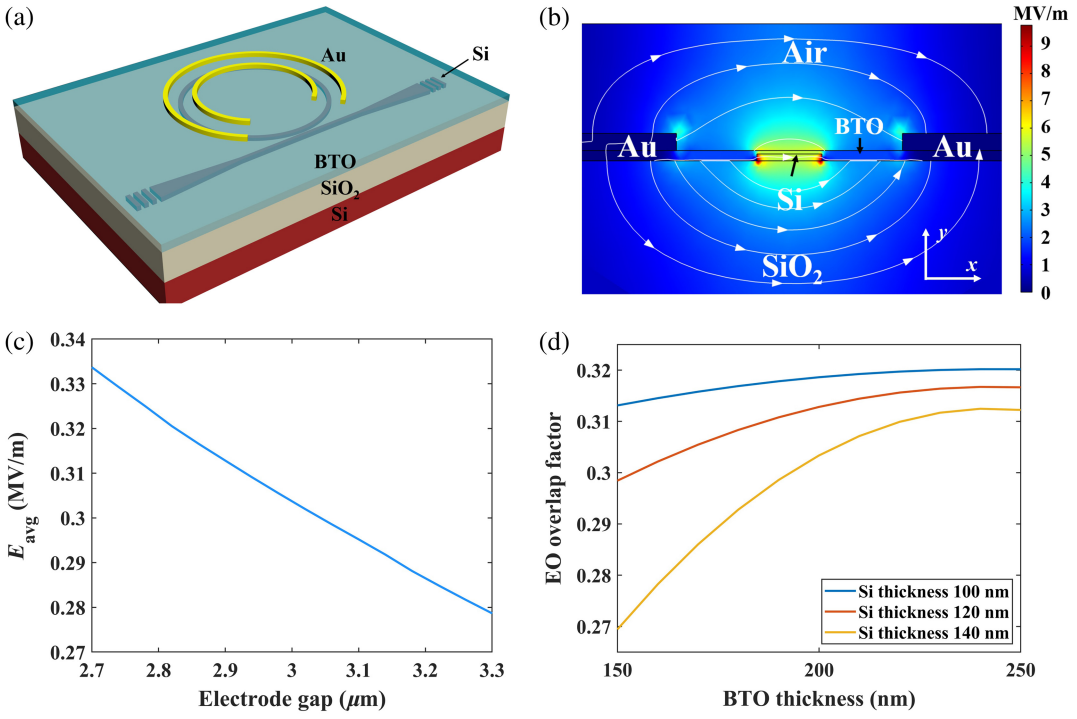

Fig. 2 (a) 3D schematic diagram of hybrid Si-BTO racetrack resonator. (b) Simulated cross-sectional static electric field distribution of hybrid Si-BTO racetrack resonator. (c) Simulated average electric field as a function of electrode gaps. (d) Simulated EO overlap factor as a function of the thicknesses of silicon layers and BTO films.

2.2 Device Fabrication and Characterization

The fabrication process of the hybrid Si-BTO devices is shown in Fig. 3(a). The patterns of gratings, waveguides, and racetrack resonators are defined on an SOI substrate with a 100-nm-thick top silicon layer using e-beam lithography (Vistec EBPG 5200 +). Then, to transfer the patterns to the top silicon layer, the inductively coupled plasma etching (SPTS DRIE-I) is utilized. After that, 150-nm-thick BTO thin film is deposited on the patterns using the CSD method. The process of the CSD method is illustrated as follows. A BTO solution (Kojundo Chemical Lab. BT-06) is spin-coated on the silicon devices at 500 revolutions per minute (rpm) for 3 s and at 4000 rpm for 40 s. Then, the deposited film is baked at 200°C for 10 min on a hot plate. The film is annealed in nitrogen (N_2) at 450°C for 5 min to increase the number of oxygen vacancies near the surface.[26] We repeat the spin-coating, baking, and annealing process 4 times to increase the BTO thickness so that the Pockels effect in BTO can be effectively utilized. During the last time, the annealing temperature is changed to 800°C to improve the crystallinity of the film.[27] After 4 times of CSD processes, the thickness of the deposited BTO thin film is measured to be about 150 nm by spectroscopic ellipsometer (Semilab SE-2000). The 300-nm-thick gold electrodes are fabricated by electron beam evaporation and patterned by the lift-off process.

Figures 3(b) and 3(c) show the scanning electron microscope (SEM) images of the BTO surface and the cross-sectional view of the Si-BTO waveguide region, respectively. The surface of the BTO film exhibits minor cracks and voids (indicated by red circles), primarily due to the rough surface and multiple repeating deposition processes. In the cross-sectional image, voids are visible at the interface between the sidewalls of the silicon

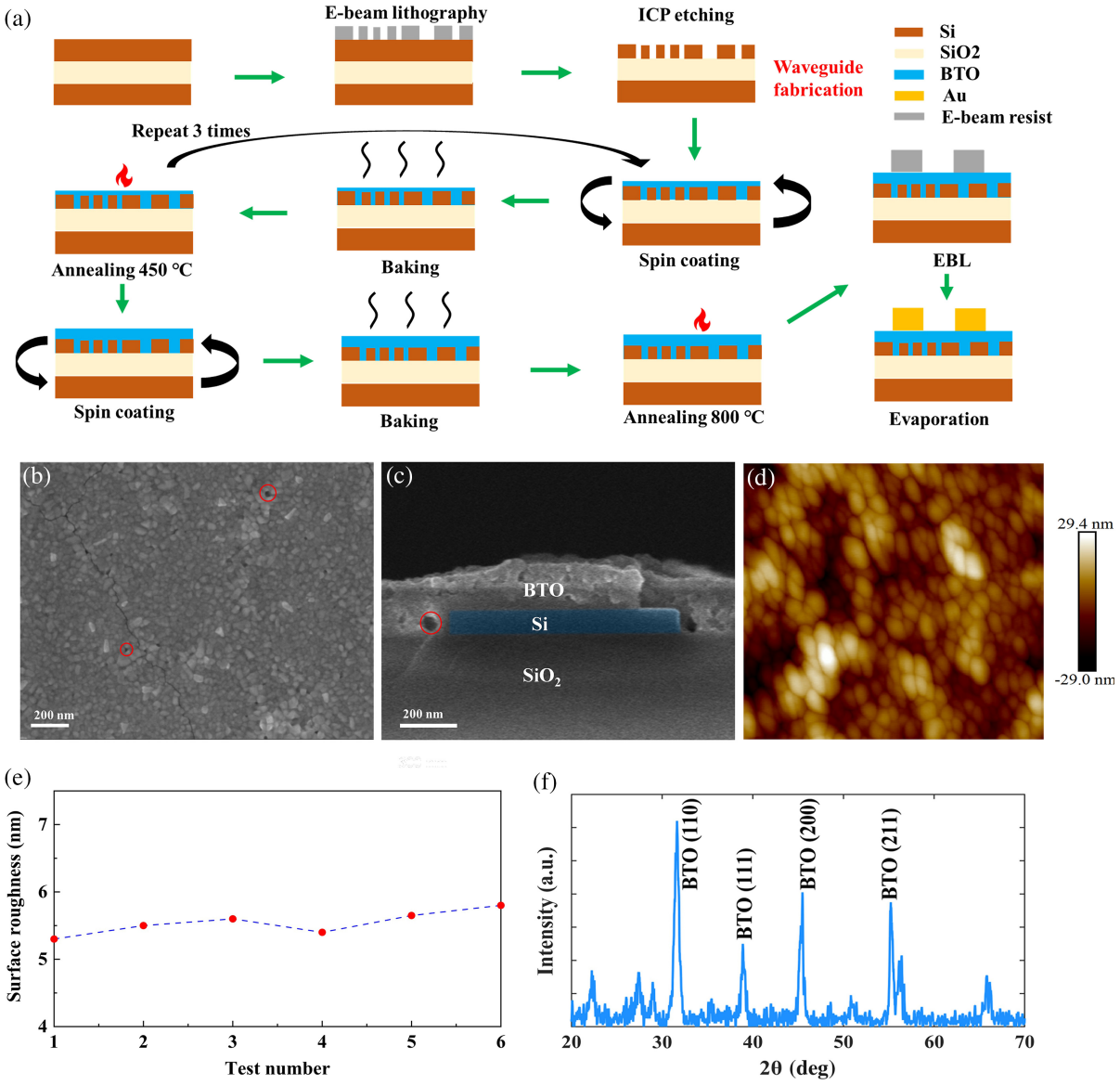

Fig. 3 (a) Fabrication process of the hybrid Si-BTO devices using the CSD method. (b) SEM photo of the surface of the BTO thin film. (c) SEM photo of the cross section of the Si-BTO waveguide region. (d) AFM on the surface of the BTO thin film. (e) Measured surface roughness across different areas. (f) XRD spectrum of the deposited BTO thin film.

waveguide and the BTO, which are attributed to the conformality of the BTO deposition. Figure 3(d) shows the atomic force micrograph (AFM) on the surface of the deposited BTO thin film. The root-mean-square surface roughness across different areas is measured through AFM after depositing BTO and is plotted in Fig. 3(e). Test numbers 1 to 3 measure the surface roughness in the waveguide region, while test numbers 4 to 6 assess the roughness near the patterns. Although the overall roughness is somewhat high (greater than 5 nm), the roughness in the waveguide region and near the patterns is numerically similar. To characterize the crystallinity of the prepared BTO film, the X-ray polycrystalline diffractometer (Brucker D8 ADVANCE) is utilized. The X-ray diffraction (XRD) spectrum is plotted in Fig. 3(f); the result reveals that the deposited film is basically polycrystalline and has a preferential orientation at (110).

3 Results

We fabricate racetrack resonators with a radius of 70 μm and a waveguide width of 0.95 μm on the hybrid Si-BTO integrated platform. To achieve a critical coupling condition, the gap between the racetrack resonator and the straight waveguide is varied from 100 to 270 nm, and the coupling length between two semicircle waveguides is varied from 5 to 35 μm. Figure 4 shows the measured transmission spectra and the Lorentz fitting of a resonance dip before and after the deposition of BTO thin film. The racetrack resonator without BTO deposited is measured to have an intrinsic quality factor Q of 107700, ER of 11.17 dB, and free spectral range (FSR) of 1.6 nm. The propagation loss is calculated as[28]

$$\alpha = \frac{2\pi n_g}{Q_{\text{int}}\lambda_0} = \frac{\lambda_0}{Q_{\text{int}} \cdot R \cdot \text{FSR}}, \tag{3}$$

where α is the propagation loss per unit length, λ_0 is the resonant wavelength, R is the equivalent radius of the racetrack resonator, and Q_{int} is the intrinsic quality factor. According to Eq. (3), the propagation loss of the silicon waveguide without BTO deposition is estimated to be 5.6 dB/cm. This loss is mainly due to the roughness of the silicon sidewalls. The estimated propagation loss of the hybrid Si-BTO waveguide is 11.3 dB/cm, which is a bit greater than the propagation loss of the waveguide without BTO deposition. The increase in losses can be attributed to the optical absorption by BTO materials and scattering due to the roughness of the BTO surface. Figures 3(b) and 3(c) show SEM images of the BTO surface and the Si-BTO waveguide cross section, revealing numerous voids and cracks. In addition, the image shows that the BTO film is polycrystalline, with grain sizes ranging from 40 to 80 nm. These features contribute to absorption losses in the material. Figure 3(e) demonstrates that the BTO surface roughness exceeds 5 nm, which can lead to scattering losses. The propagation loss can be further declined by optimizing the deposition condition, such as the annealing temperature and the annealing duration. It can be observed that the extinction ratios vary with the resonance wavelength, which is caused by the mixing of the wavelength-dependent optical mode in the coupling region.[29] The transmission spectrum of the racetrack resonator without BTO shows a slight oscillation, which originates from reflections from the grating coupler. After spin-coating the BTO thin film, the reflection from the grating

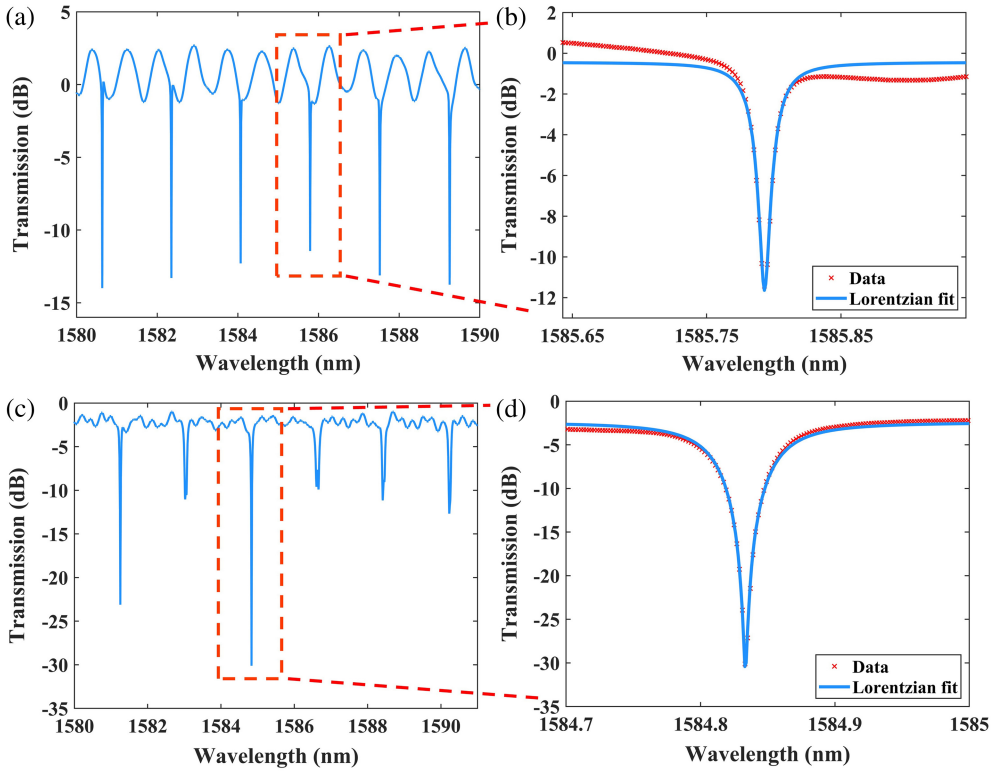

Fig. 4 (a) Measured transmission spectrum of the silicon racetrack resonator. (b) Lorentz fitting of a resonance dip of the silicon racetrack resonator. (c) Measured transmission spectrum of the hybrid Si-BTO racetrack resonator. (d) Lorentz fitting of a resonance dip of the hybrid Si-BTO racetrack resonator.

coupler is weakened and the oscillations in the transmission spectrum are reduced.

To characterize the EO performance of our hybrid Si-BTO platform, racetrack resonators with gold electrodes are fabricated. Figure 5(a) shows the optical microscope photo of the fabricated racetrack resonator; the gap between the two electrodes is 3 μm. To obtain a significant EO response for the TE optical mode, a poling step is performed by applying 30 V ($\approx$100 kV cm^{-1}) for 45 min at room temperature. The resonance shift of the transmission spectrum is plotted in Fig. 5(b); the bidirectional voltages cause the opposite movement in resonant wavelengths. Figure 5(c) presents the linear fitting between the resonance wavelength shift and the applied voltage, which yields a tuning efficiency of 6.5 pm/V. The tuning efficiency is directly relevant to the effective Pockels coefficient. To estimate the effective Pockels coefficient, we first calculate the half-wave voltage and length product to be $V_\pi L = \mathrm{L} \cdot \mathrm{FSR} \cdot \Delta V/(2 \cdot \Delta\lambda) \approx 4.51$ V $\cdot$ cm. Then, the effective Pockels coefficient can be calculated as[24]

$$r_{\mathrm{eff}} = \frac{\lambda_0}{V_\pi L n_{\mathrm{BTO}}^3 \Gamma}, \tag{4}$$

where n_{BTO} is the refractive index of BTO and Γ is the EO integral. The extracted effective Pockels coefficient is 27.2 pm/V. Although our CSD method offers a more cost-effective approach for growing BTO films, the EO coefficient obtained from this method is significantly lower than the 923 pm/V achieved in BTO single-crystal films grown using the MBE technique.[15] We attribute the small effective Pockels coefficient to the high defect density and the small grain size in the film.[15] The effective Pockels coefficient can be further optimized by improving the deposition process, for example, by extending the annealing duration and adding a template film.[21]

The leakage current across the Si-BTO racetrack resonator is measured by a semiconductor parameter analyzer (Agilent BA 1500). The measured I-V hysteresis curve is plotted in Fig. 5(d). The peaks are found at around 5/−5 V, which indicates the ferroelectric nature of the BTO thin film.[30] The power efficiency is estimated to be 2.16 pm/nW, which is comparable with HfO_2-Si microrings[31] and AlN-SiN microrings.[32] The estimated power efficiency shows an improvement of 3 orders of those tunable devices based on the conventional silicon TO approach.[33] We test and calculate the power required to achieve different resonance peak shifts in the hybrid racetrack resonator, fitting the data to a quadratic function, as shown in Fig. 5(d). Achieving a resonance peak shift of 1.7 nm is estimated to require a power consumption of 5.7 μW.

Table 1 compares the properties of BTO films produced using different deposition methods. The MBE method demonstrates good uniformity and a larger effective Pockels coefficient. Films deposited via PLD and MBE are single-crystal, while those deposited using RF sputtering and CSD are primarily polycrystalline. Unlike the MBE, PLD, and sputtering methods, which require expensive equipment and stringent preparation conditions, such as high temperature, pressure, or special gases, the CSD method is more cost-effective and flexible. BTO films can be prepared through repeated spin-coating

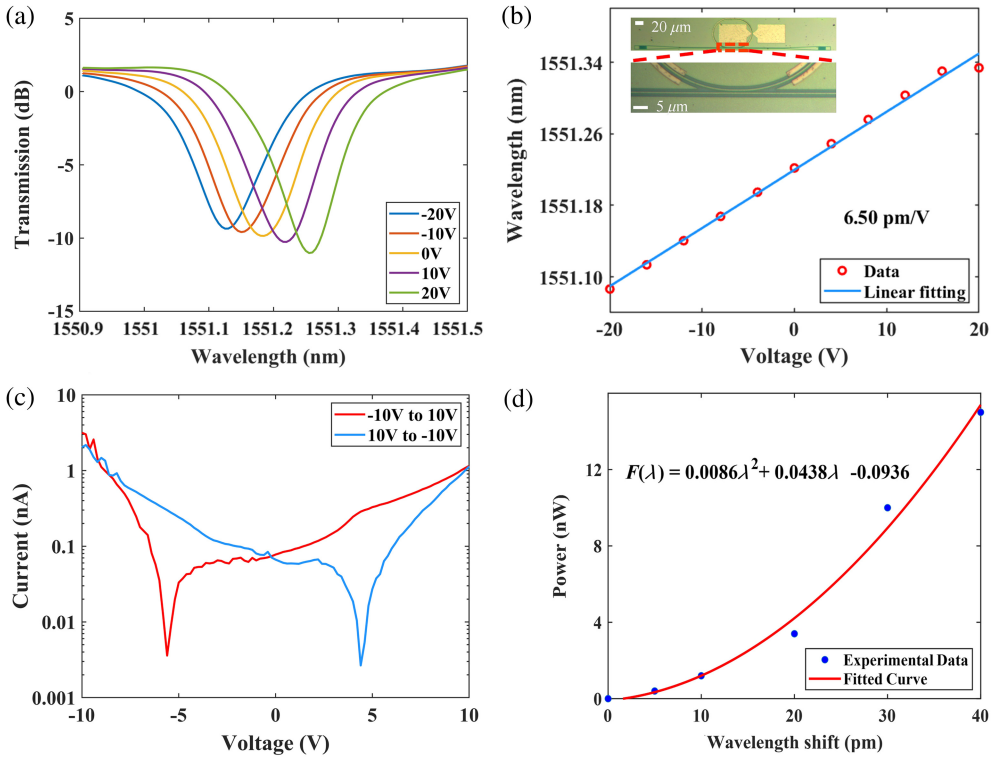

Fig. 5 (a) Measured transmission spectra when applying different voltages. (b) Linear fitting of the resonance wavelengths as a function of the applied voltages. (c) Measured I-V hysteresis curve of the fabricated racetrack resonators. (d) Power consumption as a function of resonance wavelength shift.

Table 1 Comparison between different deposition methods of BTO film.

Method	Thickness (nm)	Surface roughness (nm)	Crystalline	r_{eff} (pm/V)	Equipment cost	Fabrication process
RF sputtering[19]	102	3.1	Polycrystalline	6	High	Complex
PLD[18]	97	3.1	Single-crystal	37	High	Complex
MBE[34]	170	0.4	Single-crystal	380	High	Complex
CSD	150	5.6	Polycrystalline	27.2	Low	Simple

and annealing processes using simple spinners and annealing furnaces.

We implement experiments for high-speed tests to investigate the potential of our hybrid Si-BTO platform in optical transmission networks. The experiment framework is presented in Fig. 6(a). Eye diagrams of 30, 40, and 50 Gbps NRZ signals are measured without digital signal processing, as shown in Fig. 6(b). The bit error ratios (BERs) of the 30, 40, and 50 Gbps NRZ signal are 3.28×10^{-16}, 1.26×10^{-10}, and 1.04×10^{-4}, which are below the 7% hard-decision forward error correction (FEC) threshold of 3.8×10^{-3}. As shown in Fig. 6(c), the BERs for the 30 and 40 Gbps signals remain below the FEC threshold across various received optical power levels.

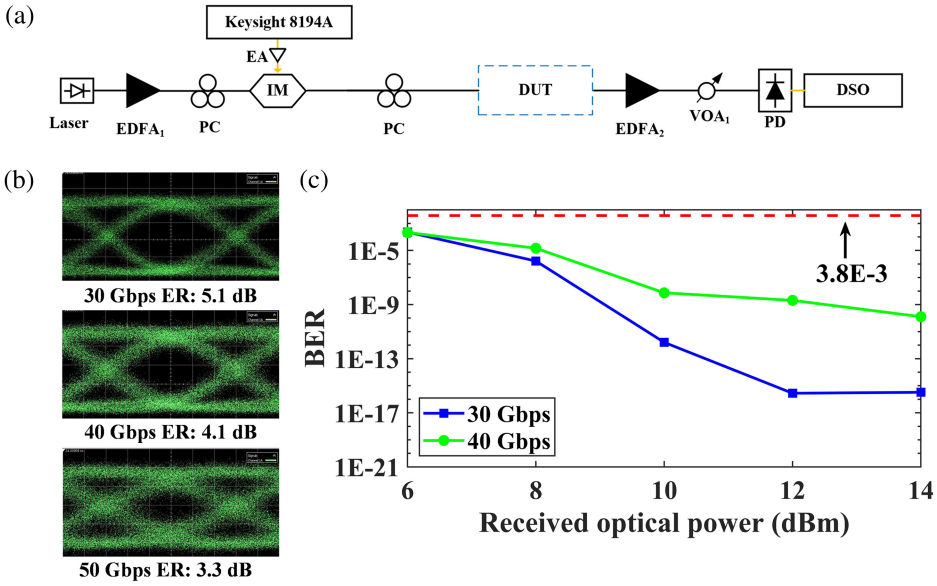

Fig. 6 (a) Experimental setup for high-speed test. EDFA, erbium-doped optical fiber amplifier; PC, polarization controller; EA, electric amplifier; DUT, device under test; PD, photodetector; DSO, digital storage oscilloscope. (b) Measured eye diagrams of NRZ signals at 30, 40, and 50 Gbps. (c) BER as a function of the received optical power.

Table 2 Performance comparison of the integrated tuning devices.

Reference	Deposition process	Tuning mechanism	Tuning efficiency (pm/V)	Power consumption (pm/nW)
Silicon[36]	—	TO	—	0.0048
Silicon[34]	—	FCPD	—	0.01
SiN-AlN[32]	Sputtering	PO	0.2	0.2
HfO_2-Si[31]	ALD	PO	8.4	7.69
BTO-SiN[11]	MBE	EO	25	23.58
LN-Si[37]	Bonding	EO	3	—
This work	CSD	EO	6.5	2.16

As shown in Table 2, we compare the performance of our Si-BTO racetrack resonators with some integrated tuning devices on different platforms. For traditional silicon tuning devices based on TO and plasma dispersion effects, the power efficiency is low (typically at the order of 0.01 pm/nW). Tuning devices based on the piezo-optic (PO) effect and Pockels effect, such as the AlN-SiN platform, HfO_2-Si platform, and BTO-SiN platform, typically have complex thin-film deposition processes. Our Si-BTO racetrack based on the CSD method provides an inexpensive and elastic alternative to achieve high-quality BTO thin films and allows easy film thickness control by repeating the spin-coating and annealing procedure. Furthermore, our device exhibits a high-power efficiency of 2.16 pm/nW which is 3 or 4 times that of the TO mechanism. Moreover, our device can support high-speed signal transmission up to 50 Gbps. However, compared to MBE-based BTO devices, our racetrack exhibits lower tuning efficiency and higher power consumption; this is mainly because the r_{eff} (~27.2 pm/V) in the CSD method is lower than that (~380 pm/V) in the MBE method. By fine-tuning the annealing temperature and duration, we anticipate achieving a higher EO coefficient in the thin film.[35]

4 Discussion

In summary, we have demonstrated a hybrid Si-BTO photonics platform using the CSD method. Unlike the MBE-based Si-BTO platform, our platform provides an easy process for the deposition of BTO film. The fabricated racetrack has a high ER of 27.9 dB and a high intrinsic quality factor of 48,000. The fabricated device exhibits a high-power efficiency of 2.16 pm/nW. Furthermore, our device is proven to transmit high-speed signals stably. The results indicate that our new Si-BTO platform based on the CSD method provides an attractive direction for low-power tuning devices.

Our hybrid Si-BTO platform shows promise for applications in EO tuning devices, but some improvements are needed for future work. First, the annealing temperature and annealing time need to be further optimized to enhance the crystallinity of the film and improve the effective Pockels coefficient. Second, to further reduce the propagation loss and allow more light to leak into the BTO layer, the deposited film can be integrated with silicon nitride. Silicon nitride has a relatively low refractive index and an ultralow loss property that can better utilize the EO properties of BTO film and realize a propagation loss of sub-1 dB. Finally, transparent conducting electrodes, such as indium tin oxide (ITO) and a smaller electrode gap, can enhance the electric field and thus increase the tuning range.

Code and Data Availability

The code and data that support the findings of this study are available from the corresponding author upon reasonable request.

Acknowledgments

This work was supported by the National Key R&D Program of China (Grant No. 2020YFB2206101) and the National Natural Science Foundation of China (Grant Nos. 62335014, 62035016, 61975115, and 61835008).

References

1. G. Wetzstein et al., "Inference in artificial intelligence with deep optics and photonics," *Nature* **588**, 39–47 (2020).
2. X. Zheng et al., "Heterogeneously integrated, superconducting silicon-photonic platform for measurement-device-independent quantum key distribution," *Adv. Photonics* **3**, 055002 (2021).
3. Y. Zhang et al., "Ultra-broadband mode size converter using on-chip metamaterial-based Luneburg lens," *ACS Photonics* **8**, 202–208 (2020).
4. Y. He et al., "Silicon high-order mode (de)multiplexer on single polarization," *J. Lightwave Technol.* **36**, 5746–5753 (2018).
5. Y. Zhang et al., "High-speed electro-optic modulation in topological interface states of a one-dimensional lattice," *Light Sci. Appl.* **12**, 206 (2023).
6. P. Kharel et al., "Breaking voltage–bandwidth limits in integrated lithium niobate modulators using micro-structured electrodes," *Optica* **8**, 357 (2021).
7. Y. Yao et al., "Performance of integrated optical switches based on 2D materials and beyond," *Front Optoelectron.* **13**, 129–138 (2020).
8. Y. Zhang et al., "Architecture and devices for silicon photonic switching in wavelength, polarization and mode," *J. Lightwave Technol.* **38**, 215–225 (2020).
9. Y. Su et al., "Silicon photonic platform for passive waveguide devices: materials, fabrication, and applications," *Adv. Mater. Technol.* **5**, 1901153 (2020).
10. D. Liang et al., "Recent progress in heterogeneous III-V-on-silicon photonic integration," *Light Adv. Manuf.* **2**, 59 (2021).
11. J. E. Ortmann et al., "Ultra-low-power tuning in hybrid barium titanate–silicon nitride electro-optic devices on silicon," *ACS Photonics* **6**, 2677–2684 (2019).
12. C. Wang et al., "Nanophotonic lithium niobate electro-optic modulators," *Opt. Express* **26**, 1547–1555 (2018).
13. X. Yan et al., "High optical damage threshold on-chip lithium tantalate microdesk resonator," *Opt. Lett.* **45**, 4100–4103 (2020).
14. K. Alexander et al. "Nanophotonic Pockels modulators on a silicon nitride platform," *Nat. Commun.* **9**, 3444 (2018).
15. W. Guo et al., "Epitaxial integration of $BaTiO_3$ on Si for electro-optic applications," *J. Vac. Sci. Technol.* **39**, 030804 (2021).
16. B. I. Edmondson et al., "Epitaxial, electro-optically active barium titanate thin films on silicon by chemical solution deposition," *J. Am. Ceram. Soc.* **103**, 1209–1218 (2019).
17. R. A. McKee et al., "Molecular beam epitaxy growth of epitaxial barium silicide, barium oxide, and barium titanate on silicon," *Appl. Phys. Lett.* **59**, 782–784 (1991).
18. M. B. Lee et al., "Heteroepitaxial growth of $BaTiO_3$ films on Si by pulsed laser deposition," *Appl. Phys. Lett.* **66**, 1331–1333 (1995).
19. C. H. Jung et al., "Reproducible resistance switching for $BaTiO_3$ thin films fabricated by RF-magnetron sputtering," *Thin Solid Films* **10**, 3291–3294 (2011).
20. P. Capper et al., "Expitaxial crystal growth: methods and materials," Springer Handbook of Electronic and Photonic Materials **1**, 1 (2017).
21. E. Picavet et al., "Integration of solution-processed $BaTiO_3$ thin films with high Pockels coefficient on photonic platforms," *Adv. Funct. Mater.* **34**, 2403024 (2024).
22. M. Burla et al., "500 GHz plasmonic Mach–Zehnder modulator enabling sub-Thz microwave photonics," *APL Photonics* **4**(5), 056106 (2019).
23. I. Taghavi et al., "Polymer modulators in silicon photonics: review and projections," *Nanophotonics* **11**, 3855–3870 (2022).
24. C. Xiong et al., "Active silicon integrated nanophotonic: ferroelectric $BaTiO_3$ devices," *Nano Lett.* **14**, 1419–1425 (2014).
25. A. Messner et al., "Plasmonic ferroelectric modulators," *J. Lightwave Technol.* **37**, 281–290 (2019).
26. S. Hashimoto et al., "Effects of final annealing in oxygen on characteristics of $BaTiO_3$ thin films for resistance random access memory," *Jpn. J. Appl. Phys.* **54**, 10NA12 (2015).

27. V. R. Chinchamalatpure et al., "Synthesis and electrical characterization of $BaTiO_3$ thin films on Si(100)," *Mater. Sci. Appl.* **1**, 187–190 (2010).
28. P. Rabiei et al., "Polymer micro-ring filters and modulators," *J. Lightwave Technol.* **20**, 1968–1975 (2002).
29. A. Griffith et al., "High quality factor and high confinement silicon resonators using etchless process," *Opt. Express* **20**, 21341–21345 (2012).
30. S. Abel et al., "A strong electro-optically active lead-free ferroelectric integrated on silicon," *Nat. Commun.* **4**, 1671 (2013).
31. J. Shen et al., "Ultralow-power piezo-optomechanically tuning on CMOS-compatible integrated silicon-hafnium-oxide platform," *Laser Photonics Rev.* **17**, 2200248 (2022).
32. H. Tian et al., "Hybrid integrated photonics using bulk acoustic resonators," *Nat. Commun.* **11**, 3073 (2020).
33. P. Dong et al., "Thermally tunable silicon racetrack resonators with ultralow tuning power," *Opt. Express* **18**, 20298–20299 (2010).
34. E. Timurdogan et al., "An ultralow power athermal silicon modulator," *Nat Commun.* **5**, 4008 (2014).
35. B. I. Edmondson et al., "Epitaxial, electro-optically active barium titanate thin films on silicon by chemical solution deposition," *J. Am. Ceram. Soc.* **2**, 1209–1218 (2020).
36. P. Dong et al., "High-speed and compact silicon modulator based on a racetrack resonator with a 1 V drive voltage," *Opt. Lett.* **35**, 3246–3248 (2010).
37. P. O. Wei et al., "Bonded thin film lithium niobate modulator on a silicon photonics platform exceeding 100 GHz 3-dB electrical modulation bandwidth," *Opt. Express* **26**, 23728–23739 (2018).

Biographies of the authors are not available.